Acoustic and high speed video analysis of exploding gas filled balloons

Michael B Muhlestein

A senior thesis submitted to the faculty of
Brigham Young University
in partial fulfillment of the requirements for the degree of

Bachelor of Science

Kent L Gee, Advisor

Department of Physics and Astronomy

Brigham Young University

April 2011

Copyright © 2011 Michael B Muhlestein

All Rights Reserved

ABSTRACT

Acoustic and high speed video analysis of exploding gas filled balloons

Michael B Muhlestein
Department of Physics and Astronomy
Bachelor of Science

Exploding gas-filled balloons are common chemistry demonstrations. They provide an entertaining and educational means to experimentally verify nonlinear acoustical theory as described by the Earnshaw solution to the lossless Burgers equation and weak-shock theory. This paper describes the theory, the demonstration, and the results of a propagation experiment carried out to provide typical results. Data analysis shows that an acetylene-oxygen balloon produces an acoustic shock whose evolution agrees well with weak-shock theory. On the other hand, the pressure wave generated by a hydrogen-oxygen balloon also propagates nonlinearly, but does not approach N-wave-like, weak-shock formation over the propagation distance. High-speed video of these explosions provide discussion material on directionality of propagating acoustic shocks. Overall, the experiment shows that popular demonstrations of chemical reactions can be extended from chemistry classrooms to a pedagogical tool for the student of advanced physical acoustics.

Keywords: nonlinear, acoustics, shock waves

ACKNOWLEDGMENTS

I was supported by a Brigham Young University Mentoring Environment Grant. I would like to thank Gordon L. Nielson and Julia A. Vernon for their help with the experiments. I would also like to thank my advisor, Dr. Gee and also Dr. Macedone for the extensive help that they contributed to this thesis. Finally, as much of this thesis is also included in a peer reviewed article, I would like to thank the reviewers for their many insights.

Contents

List of Figures

Chapter 1

Acoustic Exploding Balloon Model

The field of nonlinear acoustics is intense in every sense of the word. This field is the study of sound when the small signal approximation breaks down. Many problems in nonlinear acoustics, unlike linear acoustics, do not have analytic solutions. Even numeric schemes are often cumbersome or incomplete. Experimental acousticians also face the challenge of dealing with extremely loud sound from powerful sources. Thus it is particularly challenging to find an accessible demonstration which will both educate and bring the actuality of nonlinear acoustics to students' minds. This thesis presents such a demonstration.

The demonstration presented here is of an exploding gas-filled balloon. This classic chemistry demonstration turns out to be an extremely loud sound source which can be handled in a typical college or university. The predicted pressure waves are analytically solvable using nonlinear acoustical theory. Thus this demonstration becomes useful both for verifying nonlinear theory and as a pedagogical tool.

The demonstration consists of a balloon filled with a stoichiometric mixture of gaseous acetylene and oxygen. When ignited this creates an acoustic shock wave which cannot be described using linear acoustics. Pressure waveforms recorded with microphones placed at various distances can be analyzed and compared with theory. This demonstration is particularly useful in that it

explains principles in a more advanced field of physics, such as waveform steepening and weak-shock theory, for which classroom demonstrations are not abundant. In addition to giving insight, the entertaining nature of the demonstration can also provide motivation for introductory students to pursue more advanced studies. The demonstration can be presented along with real-world applications of acoustic shocks, including sonic booms, [1] military jet aircraft noise, [2] explosions, [3] Gatling guns, [4] and lithotripsy. [5], [6]

Chapter 1 presents a theoretical analysis of the propagating sound waves, including a discussion of the Earnshaw solution to the lossless Burgers' equation and weak-shock theory. [7] In Chapter 2 a detailed description of the demonstration is given. Propagation data obtained for both the acetylene-oxygen balloon and a hydrogen-oxygen balloon are then analyzed and compared in Chapter 3. Finally, in Chapter 4 high-speed video of the reaction is presented and discussed.

1.1 Propagation Model

Theory is a wonderful source of homework exercises and a motivation for laboratory work. Throughout this section fundamental principles of physical acoustics, as they relate to the balloon demonstration, are reviewed. Elements of the theoretical development could be given to an advanced acoustics class as a homework problem.

In order to model the propagation of the transient acoustic pulse generated by a compact explosive source, two models are necessary: a model equation that appropriately describes the evolution of the pressure waves and a model for the source pressure waveform. The use of the source waveform in the propagation model, which relies on the Earnshaw solution to the lossless Burgers' equation and weak-shock theory, results in theoretical expressions that can be used to compare with experimental data obtained from the demonstration.

1.1.1 The Earnshaw Solution to the Burgers' Equation

This section describes the theory that is used to model the continuous portion of the propagating transient. As this theory is not original and our development is similar to that of Blackstock et al., [7] it is largely included for completeness in this pedagogical thesis. In addition, although our demonstration involves the propagation of finite-amplitude spherical waves, it is easier to develop the plane-wave solution and then convert it into spherical coordinates afterwards, as done by Blackstock et al. [7]

The model equation used to describe the nonlinear evolution of the acoustic pressure, p, (hereafter just called the pressure), is the lossless, planar Burgers' equation

$$\frac{\partial p}{\partial x} = \frac{\beta}{\rho_0 c_0^3} p \frac{\partial p}{\partial \tau} \tag{1.1}$$

where x is the distance from the source, β is the parameter of nonlinearity (1.201 for air), ρ_0 is the ambient density, c_o is the small-signal sound speed. The retarded time τ is related to time t via $\tau = t - x/c_0$. The planar Burgers' equation is valid for continuous waveforms, which means that once shocks form it no longer describes the entire wave. A physical interpretation of this equation is that high pressure portions of the waveform (peaks) propagate supersonically while low pressure portions (troughs) propagate subsonically.

An often used solution to the lossless Burgers' equation (derived in Appendix A) was developed by Earnshaw [7] and may be written as [7]

$$p = f(\phi) \tag{1.2}$$

$$\phi = \tau + \frac{\beta x p}{\rho_0 c_0^3} = \tau + \frac{\beta x}{\rho_0 c_0^3} f(\phi) \tag{1.3}$$

where $f(\phi)$ when $x = 0$ is the source pressure as a function of time. The variable is the nonlinearly distorted time scale and is called the Earnshaw phase variable by Blackstock et al. [7] In addition to facilitating analytical solutions, the Earnshaw solution is very convenient for numerical solutions

of the Burgers' equation [8] [9] [2] as the initial waveform values do not change, but only the time at which they occur changes. Physically, the pressure-dependent distortion of the Earnshaw solution in Eq. (1.3) describes how the compressions travel faster than rarefactions in the waveform steepening process prior to shock formation.

The Earnshaw solution can be used as a pedagogical tool or as part of a homework exercise where students can use the solution to distort a discretely sampled waveform. For example, the Earnshaw solution can be used as an alternative to (or comparison with) the Fubini series solution [10] for a monofrequency source described by $f(\phi) = p_0 \sin(\omega\tau)$, where ω is the angular frequency, so by Eq. (1.3) $\phi = \omega\tau + \beta p_0 \omega x \sin(\phi)/\rho_0 c_0^3$. Plotting the solution to the pressure as a function of the nondimensional distance $\sigma = \beta p_0 \omega x/\rho_0 c_0^3$ is instructive. The results for four values of τ are displayed in Fig. 1.1.

Notice in Fig. 1.1 that the waveform becomes perfectly vertical at $\sigma = 1$, thus forming the first shock. For this reason $\sigma = 1$ is referred to as the shock formation distance, and σ the distance relative to the shock formation distance. Having students plot the solution for $\sigma > 1$ can be used to motivate a discussion of weak-shock theory and the equal-area rule. [7] An example has been included in Fig. 1.1 for $\sigma = 2$, with the vertical line denoting the location of the shock.

1.1.2 Weak-Shock Theory

For distances such that $\sigma > 1$, the continuous Earnshaw solution cannot be used in the multivalued regions. Weak-shock theory is instead required. Weak-shock theory is based on three assumptions. First, shocks are "weak", which is described further below. Second, losses are only considered at the shocks (i.e. the propagation of the continuous portion of the waveform may be considered lossless). Third, shocks are discontinuities.

Using these assumptions with the Rankine-Hugoniot shock relations, [11] one finds that shocks

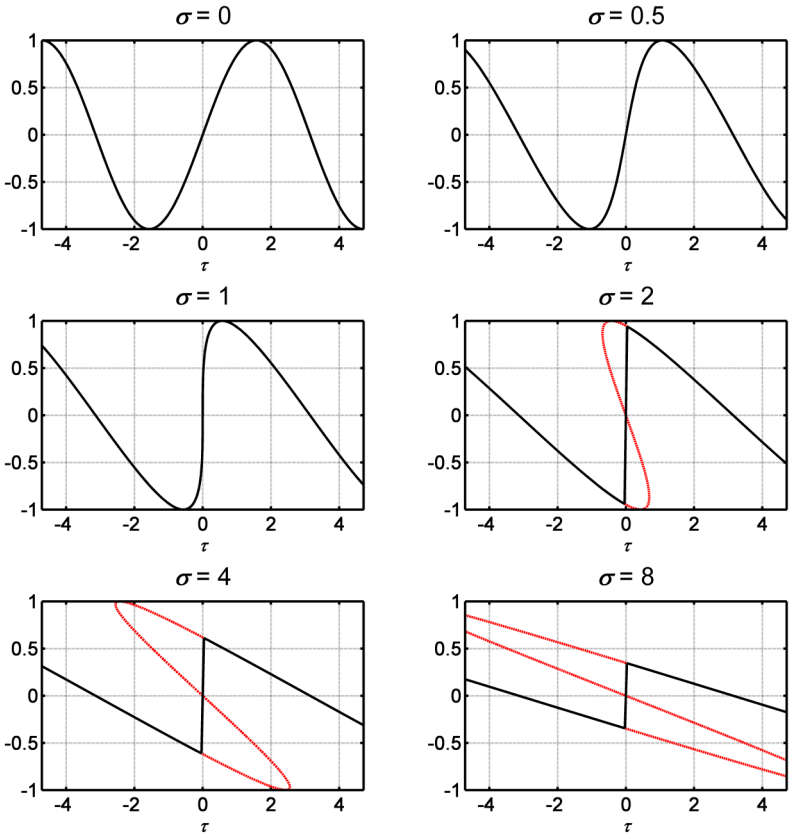

Figure 1.1 Nonlinear propagation of an initially sinusoidal wave of frequency ω according to the Earnshaw solution to the planar, lossless Burgers' equation. The variable σ is dimensionless distance where $\sigma < 1$ represents the preshock region. The multivaluedness of the Earnshaw-derived pressure for $\sigma > 1$ can be used to motivate a discussion of weak-shock theory. The amplitude has been normalized (p/p_0).

propagate at a velocity of

$$v_{sh} = -\frac{\beta}{\rho_0 c_0}\frac{(p_a + p_b)}{2} \tag{1.4}$$

where v_{sh} is the velocity of the shock, and p_a and p_b are the pressure ahead of the shock and behind the shock, respectively. Note that this means that shocks propagate at speeds different from the continuous portions of the waveform surrounding the shock. In order to find the location of a shock the relation for the retarded speed of the shock

$$\frac{\partial \tau_{sh}}{\partial x} = -\frac{\beta}{\rho_0 c_0^3}\frac{(p_a + p_b)}{2} \tag{1.5}$$

is a more useful form of Eq. (1.4), where τ_{sh} is the retarded time of arrival of the shock. In order to use Eq. (1.5), p_a and p_b are found using the Earnshaw solution, Eqs. (1.2) and (1.3).

$$\begin{aligned} p_a &= f(\phi_a), \qquad \phi_a = \tau + \tfrac{\beta x p_a}{\rho_0 c_0^3} \\ p_b &= f(\phi_b), \qquad \phi_b = \tau + \tfrac{\beta x p_b}{\rho_0 c_0^3} \end{aligned}. \tag{1.6}$$

Implicit in the use of Eq. (1.6) is the use of the equal area rule, a consequence of weak shock theory. This rule is that the shock separates equal areas as defined by the Earnshaw solution (as can be seen in Fig. 1.1). Equations (1.2,1.3,1.6) are an adequate model set of equations to describe the finite-amplitude pressure wave propagation.

As with any model, it is important to understand the limitations of weak-shock theory. One of the three assumptions discussed above is that shocks are "weak." Temkin [12] studied errors associated with the weak-shock approximation in the expression for the entropy change across shocks in planar sawtooth waves at sea level. Used as the figure of merit was the shock strength, defined as

$$\delta = \frac{p_b - p_a}{p_b + p_{amb}}, \tag{1.7}$$

where p_{amb} is the ambient pressure. The upper bound of acceptable errors was found to be $\delta = 0.1$, which corresponds to an rms sound pressure level of 165 dB re 20 μPa. Note that Blackstock [13] used a different criterion in his examination of weak-shock theory limits. He employed the peak

acoustic Mach number, $M = u_0/c_0$, where u_0 is the peak particle velocity, with "weak" being defined as $M < 0.1$. This yields an upper bound for planar sawtooth waves of 174 dB re 20 μPa ($\delta = 0.329$). [14]

Regardless of the criterion used to obtain the weak-shock theory upper bound, neither result applies strictly to the waveform of an exploding gas-filled balloon. One cause is geometric spreading, which serves to rapidly reduce the peak pressure for the same propagation range. This would effectively increase the upper bound of weak-shock theory. Another cause is the nature of the waveform itself, which is an asymmetric transient rather than a symmetric, stationary signal. To the authors' knowledge, the theoretical upper limits of weak-shock theory for a spherically propagating transient impulse have not been determined as has been done for the planar sawtooth wave. Therefore, the appropriateness of the weak-shock theory model for this case is established empirically by the level of agreement between predictions and experiment.

1.2 Explosion Model

A commonly used model for an acoustic impulse created by an explosion is the modified Friedlander equation11, written as

$$p(t) = p_s^+(1 - t/T^+)e^{-bt/T^+}, \tag{1.8}$$

where p_s^+ is the peak shock pressure value, T^+ is duration for which the pressure value is positive and b is a fitting parameter. However, this equation is not as well suited for analytical analysis as a shock followed by an exponentially decaying tail, which is sufficient to illustrate the features of interest. Thus,

$$f(t) = \begin{cases} p_0 e^{-t/t_0} & t > 0 \\ 0 & t < 0 \end{cases}, \tag{1.9}$$

where p_0 is the initial amplitude of the shock and t_0 is the initial e-1 decay time of the tail. Note that $\tau = t$ for $x = 0$. The problem of solving Eqs. (1.2 - 1.6) with Eq. (1.9) as the source was previously

solved with a finite-difference formulation by Rogers. [15] Blackstock [16] approached it by an analytical formulation and found expressions for many key elements though he did not provide a solution for the entire pressure waveform. The present formulation is included for educational value, as it solves the problem completely from the Earnshaw solution and weak-shock theory perspective.

There are two semi-infinite portions of the wave that are continuous: before the shock and after the shock. Because $p = 0$, the Earnshaw phase variable is simply $\phi = \tau$ before the shock. For the portion behind the shock, the Earnshaw solution yields

$$p = p_0 e^{-(\tau + Cxp)/t_0}. \tag{1.10}$$

where the substitution of $C = \beta/\rho_0 c_0^3$ is made. Equation (1.10) can be rewritten as

$$ze^z = \frac{p_0}{t_0} Cxe^{-\tau/t_0} \tag{1.11}$$

where $z = Cxp/t_0$. The solution to Eq. (1.11) is

$$z = W\left(\frac{p_0}{t_0} Cxe^{-\tau/t_0}\right), \tag{1.12}$$

where W is the Lambert W function. [17] Equation (1.12) in conjunction with Eq. (1.9) implies that

$$p(x,\tau) = \begin{cases} \frac{t_0 W\left(\frac{p_0}{t_0} Cxe^{-\tau/t_0}\right)}{Cx} & \tau > \tau_{sh} \\ 0 & \tau < \tau_{sh} \end{cases}, \tag{1.13}$$

As mentioned above, Eq. (1.13), which is derived from the Earnshaw solution, is only valid for continuous portions of the waveform, and weak-shock theory is necessary to find τ_{sh} in terms of x. This requires that Eqs. (1.5) through (1.6) be solved. The source waveform allows one to immediately see that $p_a = 0$. This means that the peak pressure of the shock (p_{sh}) is identical to p_b. Solving for p_{sh} in a functional form is more difficult (and is likely worthy of a graduate-level homework exercise; see Appendix B) but Blackstock [16] found it to be

$$p_{sh} = \frac{\sqrt{1 + 2p_0 Cx/t_0} - 1}{Cx/t_0}. \tag{1.14}$$

Once p_{sh} is found, Eqs. (1.2) and (1.3) evaluated at ϕ_{sh} allow τ_{sh} to be found:

$$\tau_{sh} = t_0 - t0\sqrt{1+2p_0Cx/t_0} - t_0 \ln\left(\frac{\sqrt{1+2p_0Cx/t_0}-1}{p_0Cx/t_0}\right). \tag{1.15}$$

Figure 1 illustrates how the waveform spreads as it propagates as Eqs. (13) through (15) predict. Because the Lambert W function can not be written in terms of elementary functions, an approximation is necessary. Rogers [15] used Newton's method to find an approximation for the pressure wave in terms of elementary functions. To generate the results in Fig. 2, the MATLAB® lambertw.m25 function was used.

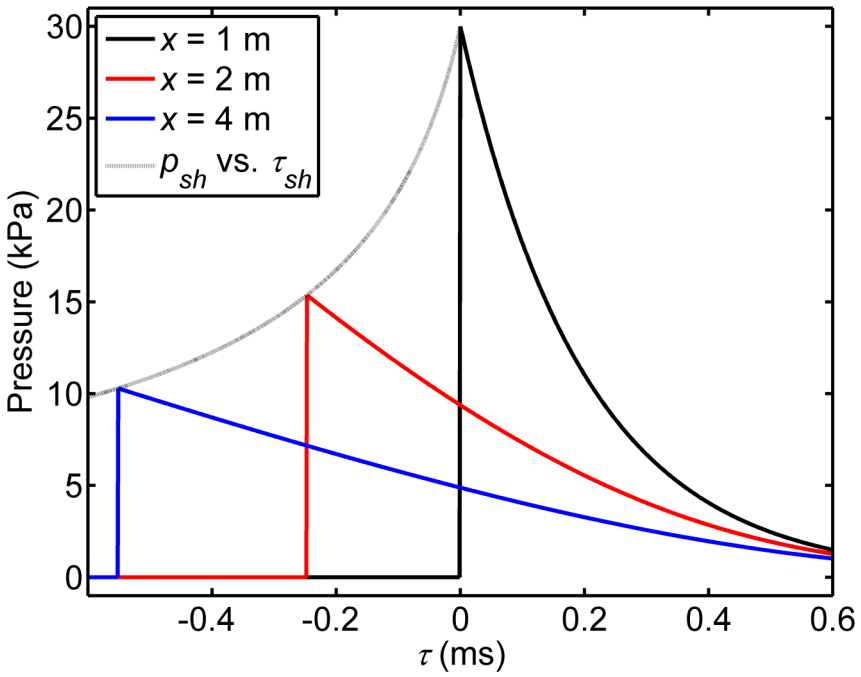

Figure 1.2 Theoretical evolution of a propagating planar shock with exponential tail. In this case, t_0 is approximately 0.2 ms and $p_0 = 30$ kPa. The choice of p_0 is derived from the acetylene-oxygen balloon experiment.

Equations (1.13) and (1.14) provide a full profile of the pressure evolution of this plane-wave model. In order to convert this result into spherical coordinates, Eq. (1.13) is multiplied by r_0/r and in Eqs. (1.13) and (1.15) x is replaced with $r_0 \ln(r/r_0)$, where r_0 is the reference radius at which

p_0 and t_0 are known and r is the radius from the source. Thus the expressions for $p(x,\tau)$ and τ_{sh} in spherical coordinates are

$$p(r,\tau) = \begin{cases} \frac{r_0 p_0}{r} \frac{t_0 W\left(\eta \ln(r/r_0) e^{-\tau/t_0}\right)}{\eta \ln(r/r_0)} & \tau > \tau_{sh} \\ 0 & \tau < \tau_{sh} \end{cases}, \tag{1.16}$$

$$t_{sh} = t_0 - t_0\sqrt{1+2\eta \ln(r/r_0)} - t_0 \ln\left(\frac{\sqrt{1+2\eta \ln(r/r_0)}-1}{\eta \ln(r/r_0)}\right), \tag{1.17}$$

$$\eta = \frac{p_0}{t_0}\frac{\beta r_0}{\rho_0 c_0^3}, \tag{1.18}$$

where τ is now defined as $t-(r-r_0)/c_0$.

Also of interest is the peak pressure value in spherical coordinates, obtained by transforming Eq. (1.14) as described above. The peak pressure (p_{sh}) is given by

$$p_{sh} = \frac{r_0 p_0}{r}\frac{\sqrt{1+2\eta \ln(r/r_0)}-1}{\eta \ln(r/r_0)}. \tag{1.19}$$

Figure 2 illustrates how the waveform spreads as it propagates as Eqs. (1.16) through (1.19) predict.

It is important to remember that Eqs. (1.16) through (1.19) only describe the evolution of the shock with decaying exponential tail under conditions that satisfy weak-shock theory. In addition to the "weak" requirement described previously, for a real fluid there are many factors that can lead to discrepancy between experiment and theory. Molecular relaxation and thermoviscous absorption will cause the shock rise to no longer be discontinuous. [18], [19] Furthermore, as distance increases, the absorptive processes will result in ordinary losses affecting the entire waveform. [20] In addition, dispersion will also be an important consideration over large distances. [21]

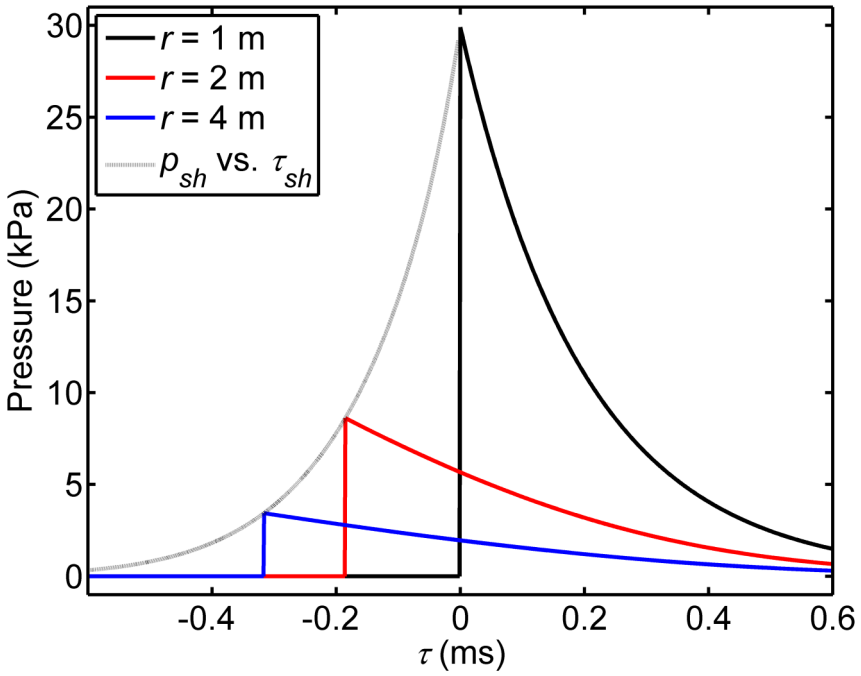

Figure 1.3 Theoretical evolution of a spherically propagating shock with exponential tail. In this case, t_0 is approximately 0.2 ms, $p_0 = 30$ kPa and $r_0 = 1$ m.

Chapter 2

Experiment

This section discusses the basic chemistry associated with the exploding balloon demonstration, describes how the demonstration is carried out and then provides details of the experiment to compare with the theory described in the previous section.

2.1 Explosion Chemistry Overview

Nonlinearly propagating pressure waves can be generated by chemical reactions in the combustion of two easily obtainable fuels: hydrogen (H_2) and acetylene (C_2H_2). In any chemical reaction, reactant species experience a rearrangement of atoms or ions to make new product species. During chemical reactions, bonds between atoms are broken, with new bonds then formed to generate product species. The total energy change for the reaction is the difference between the energy required to break bonds and the amount of energy released in the formation of new bonds. In the case of the combustion reactions described here, one important result of the reaction is a net release of energy; more energy is released in the forming of new more stable bonds than was required to initially break the bonds between reactant species.

One measure for the amount of energy released in a reaction is enthalpy change (ΔH°); enthalpy

is a measure of the heat energy in a reaction. The heat energy released in a reaction will heat the reaction gases which will increase the velocity of the gas molecules generating a pressure wave at the site of the explosion. The following reactions outline the combustion reactions for the fuels we used:

$$\begin{aligned} 2H_2 + O_2 &\rightarrow 2H_2O\ (l) & \Delta H^\circ &= -285.8\ \text{kJ mol}^{-1} \\ 2C_2H_2\ (g) &\rightarrow 4CO_2\ (g) + 2H_2O\ (l) & \Delta H^\circ &= -1301.1\ \text{kJ mol}^{-1} \end{aligned} \tag{2.1}$$

The enthalpy values are negative to indicate that heat energy is released from the reaction.

Note that even though the same numbers of fuel moles are used in each of the two reactions, there is a significant difference in the enthalpy change in these two gases. The reason for this is not that more bonds are formed than are broken. In fact, the same numbers of bonds are broken as are formed in each case. The disparity in energy between the two reactions in Eq. (2.1) arises from differences in the types of bonds which are formed. About twice as much energy is released in the formation of a carbon-oxygen bond as in a hydrogen-oxygen bond. While considerations of enthalpy alone do not account for differences in reaction rate, it is important to consider the energy differences between these two reactions. However, a complete discussion of the reaction kinetics of these two reactions is beyond the scope of this article.

2.2 Demonstration Description

2.2.1 Balloon Preparation

For preparation the balloons, the reactions (2.1) were used to determine the appropriate amount of oxygen (O_2) for a complete burn of the fuel. For combusting hydrogen (H_2), 0.370 moles of hydrogen with 0.185 moles of oxygen was used (with total balloon diameter of 31.1 cm). For acetylene combustion, 0.057 moles of acetylene with 0.143 moles of oxygen was used (with total balloon diameter of 22.1 cm). The amount of fuel used in these experiments was a matter of con-

venience; however, accurate delivery of gases is difficult. In practice, the volume of gas required was converted to the diameter of a sphere. Because balloon shape could affect the combustion process and the shape of the acoustic impulse, we used latex balloons which were manufactured to be more spherical than typical tear-drop shaped party balloons. Plastic tubing was shaped to form a ring of the diameter required for a certain volume calculated by the ideal gas law. Balloons were then filled directly from compressed gas cylinders until the balloon walls just touched the inside diameter of the plastic ring. Two plastic tubing rings were prepared: a smaller ring to ensure the proper amount of fuel, and a second larger ring to indicate the amount of oxygen to be added to the initial amount of fuel to create the appropriate mixture.

In order to prevent the initial acoustic impulse and reflections from overlapping in time, the distance from the explosion to any hard surfaces should be greater than 30 cm. This distance is calculated from the measured A durations (duration of initial overpressure from impulses) of the explosions at the 3.46 m microphone. This will allow for clear analysis from an experiment conducted in a regular classroom (not just in an anechoic chamber, as used in this experiment).

2.2.2 Safety Precautions

Once the mixture is prepared, precautions should be observed: (1) Double hearing protection should be worn once the mixture is ready. (2) Eye protection should be worn to protect the presenter and nearby viewers from flying bits of balloons. Whatever mechanism is used to anchor the balloon should be secured so that it will not become a projectile. The fireball created by the explosion is approximately 80 cm in diameter (see Fig. 2.2). Fire hazards should be considered; do not ignite the balloon within 2 m of flammable surfaces.

Balloons are ignited by using a homemade device consisting of surgical tubing attached to a 1 m hollow stainless steel rod. The surgical tubing is then connected to a natural gas supply and the device is used as a "flame wand" to ignite the balloon. When initiating the reaction,

presenters should hold the flame wand with an outstretched arm to maintain a 6' distance from the explosion. Also, as a practical note, acetylene balloons should be used within about 20 minutes after preparation as the acetylene diffuses through the latex balloon wall at a sufficiently fast rate that reproducibility and balloon volume are reduced.

Another consideration in performing the demonstration is the potential for auditory hazard. In order to observe nonlinear effects of sound, potentially dangerous levels of sound are needed that require proper protection for those involved. Recent experiments on the levels generated by hydrogen-oxygen balloons have been discussed by Gee et al. [22] To reduce the peak levels below 140 dB re 20 μPa for the demonstrator, double hearing protection is worn. This can provide approximately 50 dB of attenuation for impulse noises. [23] Due to the explosive nature of the demonstration and the potential for balloon piece projectiles, a lab coat, and eye protection should also used by the person lighting the balloons.

2.3 Balloon and Microphone Setup

The acetylene-oxygen balloon was used to demonstrate the nonlinear spherical spreading of a shock with an initially exponential tail. [3] In order to focus on spherical spreading and minimize other effects due to reflections the experiment was conducted in the large fully anechoic chamber at Brigham Young University with working dimensions of 8.71 $\times$ 5.66 $\times$ 5.74 m. It should be noted that the anechoic chamber has an upper frequency limit ($\sim$20 kHz) for which it is anechoic. This means that some reflections from the room at the very high frequencies associated with shocks are unavoidable, but these reflections do not impact the shock characteristics of primary importance to this thesis (see Section 2.2.1).

As shown in Fig. 2.1, microphones were placed at 1.03 m, 1.18 m, 1.33 m, 1.64 m, 1.94 m, 2.85 m, and 3.46 m from the center of the balloon for the acetylene and oxygen balloon test. For the

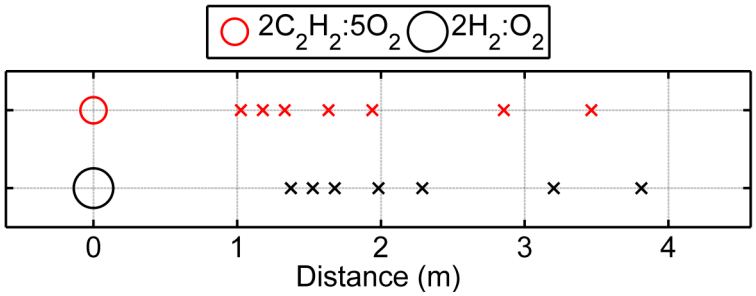

Figure 2.1 Schematic showing microphone locations relative to the acetylene-oxygen ($2C_2H_2$:$5O_2$) and hydrogen-oxygen ($2H_2$:O_2) balloons for the results described in this thesis.

hydrogen and oxygen balloon test, the balloon was 0.305 m (1.00 ft) farther from all of the microphones. As this is not necessarily the exact source location, the value of r_0 is a source of potential error. The microphones were suspended from a network of cotton twine strung between two stands in order to minimize the number of possible scattering sources. The microphones used were 3.18 mm (1/8 in) G.R.A.S. 40DD microphones, except for the most distant microphone which was a 6.35 mm (1/4 in) G.R.A.S. 40BD microphone. The grid caps of the microphones were removed in order to remove any shock-induced high-frequency resonances of the cavity between the grid cap and the microphone diaphragm. [24] Because the microphone orientation has a significant effect on the measurements of shock amplitude [24], [25], the microphones were placed as near as possible to grazing incidence. Uncertainty in the orientation and any shadowing and scattering from upstream microphones is one source of error in the measurement of the shock amplitude.

During the experiments, time waveform data were acquired with a National Instruments PXI-based system using 24-bit PXI-4462 cards controlled by LabVIEW-based software. The data were acquired at a rate of 204 800 samples per second (4.9 μs per sample). Post processing of the data was done using MATLAB®.

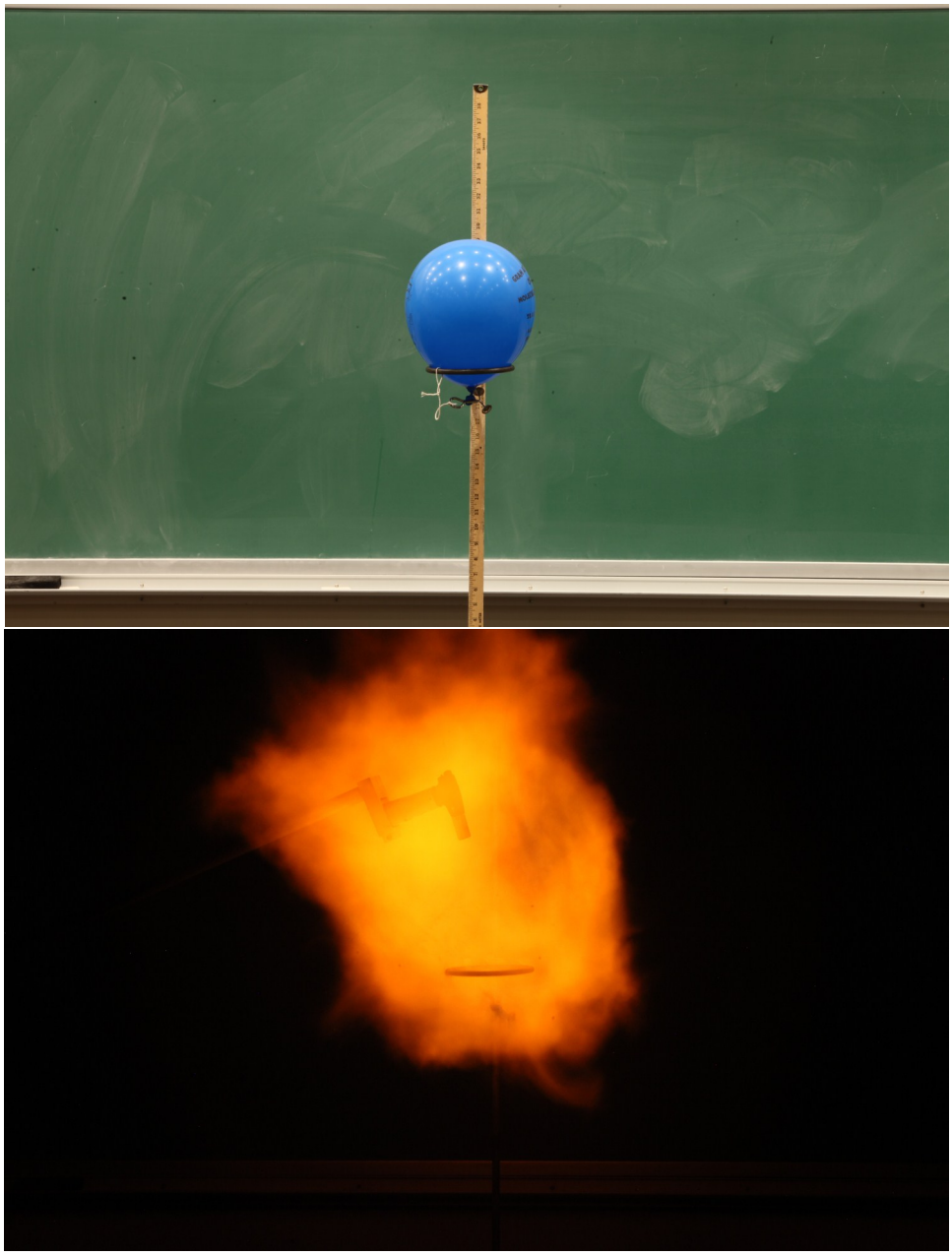

Figure 2.2 Before (above) and during (below) pictures of an acetylene-oxygen balloon explosion. The ruler in the before picture is present for scale. The maximum explosion radius is about 79 cm.

Chapter 3

Data Analysis

3.1 Experiment Results

Shown in this section are time waveform measurements for both the acetylene-oxygen and hydrogen-oxygen balloons. Presented in Fig. 3.1 is the acetylene-oxygen balloon waveform aligned at the zero crossing, which propagates at the ambient speed of sound and thus does not change with regard to the retarded time. The peak pressure, p_{pk}, of the acetylene-oxygen balloon at 1.02 m was 31.03 kPa. This is equivalent to 183.8 dB re 20 μPa, using $L_{pk} = 20log10(p_{pk}/p_0)$, where L_{pk} is the peak sound pressure level.

The peak pressure for the hydrogen-oxygen balloon shown in Fig. 3.2, 3.26 kPa (164.2 dB re 20 μPa), is substantially less than that of the acetylene-oxygen balloon at 1.17 m, 23.8 kPa (181.5 dB re 20 μPa), and occurs over a greater time scale. Aligning the initial impulse also aligns the waveform at the zero crossing, as shown in Fig. 3.2, below. Comparing Fig. 3.2 to Fig. 3.1 shows that this dual alignment, or lack of time-scale elongation, is a major difference between the two explosions, as is the lack of a significant shock in Fig. 3.2.

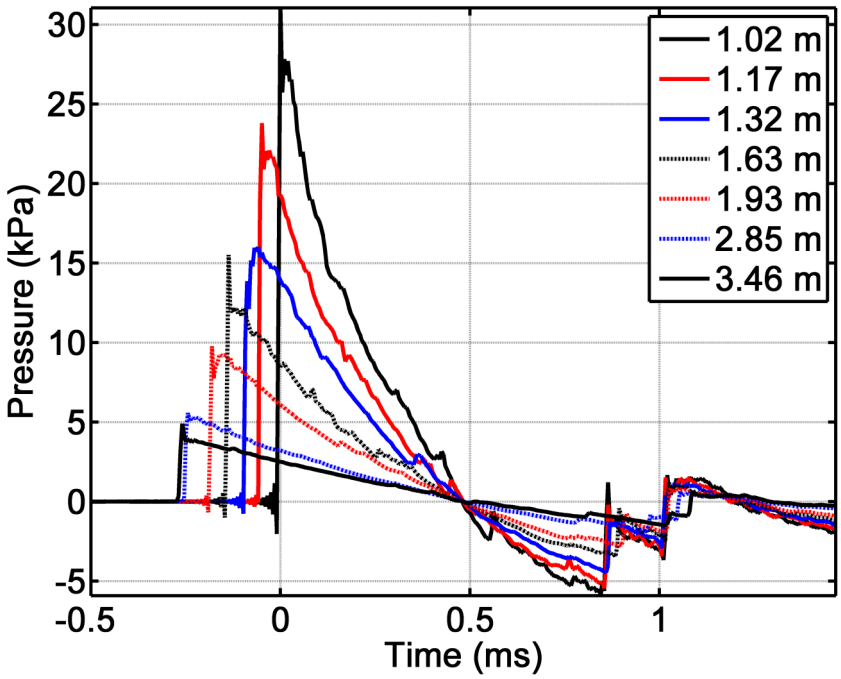

Figure 3.1 Measured pressure-time waveforms, aligned at the impulse zero crossing, for an acetylene-oxygen balloon.

3.2 Analysis and Discussion

The results of the above section provide for interesting discussion as to the effects of shocks and nonlinear propagation appropriate for an advanced acoustics course. It is first important to put the acetylene-oxygen balloon peak levels in context with the limits of weak-shock theory, given that a reasonably sized balloon filled with readily available gasses can produce levels exceeding 180 dB at close range. Calculation of the shock strength in Eq. (1.7) for the acetylene-oxygen balloon at the closest microphone yields $\delta = 0.341$. This is greater than the upper limit of weak shock theory ($\delta = 0.1$) suggested by Temkin. [12] However, as mentioned above, these limits are specifically for periodic, planar waves. Regardless, comparing the data with the weak-shock theory is still a valuable exercise, as is shown below.

The theory of a propagating weak shock with an exponential tail predicts that the peak ampli-

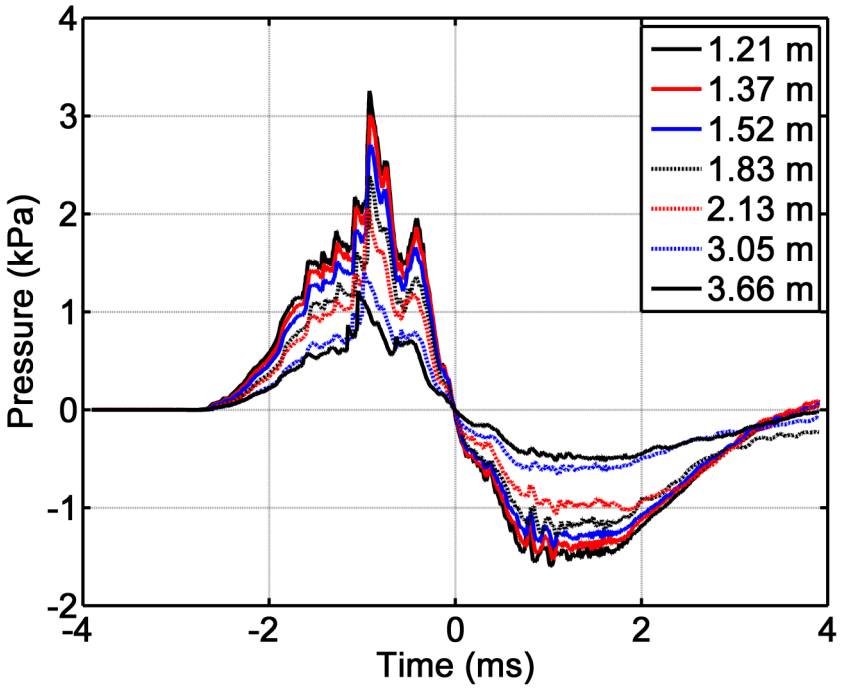

Figure 3.2 Measured pressure-time waveforms for a hydrogen-oxygen balloon.

tude (p_{sh}) rolls off according to Eq. (1.19) and its retarded time of arrival (τ_{sh}) evolves according to Eq. (1.17). Because the zero crossing travels at the ambient sound speed and its retarded time does not change, it is a useful reference point from which to examine this waveform time-scale increase. To compare with experiment, Eqs. (1.17) and (1.19) require values for r_0, p_0, and t_0. The value for r_0 used is the distance from the source, approximated as the center of the balloon, to the first microphone. The values of p_0 and t_0 are taken directly from the measured data. The peak pressure of the closest microphone is used as p_0 and the time it takes for the pressure to decay to $1/e$ of the peak value is used for t_0.

In Fig. 3.3, the peak pressures from Fig. 3.1 are displayed along with the theoretical nonlinear prediction of the peak value roll-off over distance from Eq. (1.19). Ordinary spherical spreading is also included for reference. Inspection of Fig. 3.3 shows that the experimental data diverge quickly and substantially from the linear theory. This means that in order to get any sort of reasonable

prediction for the peak pressure value, nonlinear theory must be used. At 3 m from the source, the excess attenuation of the peak is greater than 6 dB.

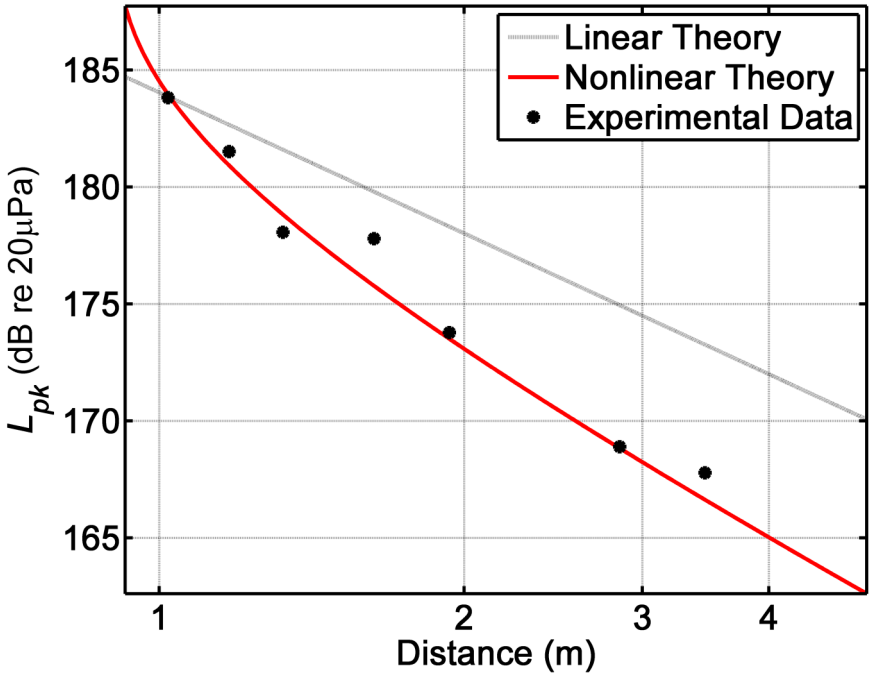

Figure 3.3 Measured peak sound pressure levels (L_{pk}) from the acetylene-oxygen balloon as a function of distance with theoretical linear (for comparison) and nonlinear curves.

Figure 3.4 shows the measured time waveforms from Fig. 3.3 with respect to retarded time with the zero crossing as a reference point. Although the experimental p_{sh} vs. τ_{sh} evolution general agreement with Eqs. (1.16) through (1.18) is noted, there are differences that were fairly consistent for all balloon explosions measured. Examination of the time waveforms and comparison with data shown by Gabrielson et al. [24] suggests that the inexactness in the peak pressure measurement is primarily due to slight pressure microphone orientation errors.

At the base of the shocks in Fig. 3.4 are pressure oscillations. These are artifacts of the digital to analog converter used in this experiment and is a consequence of the Gibbs effect. These oscillations may also exist at the top of the shocks as well, which may cause some small overestimation

of the peak pressure values.

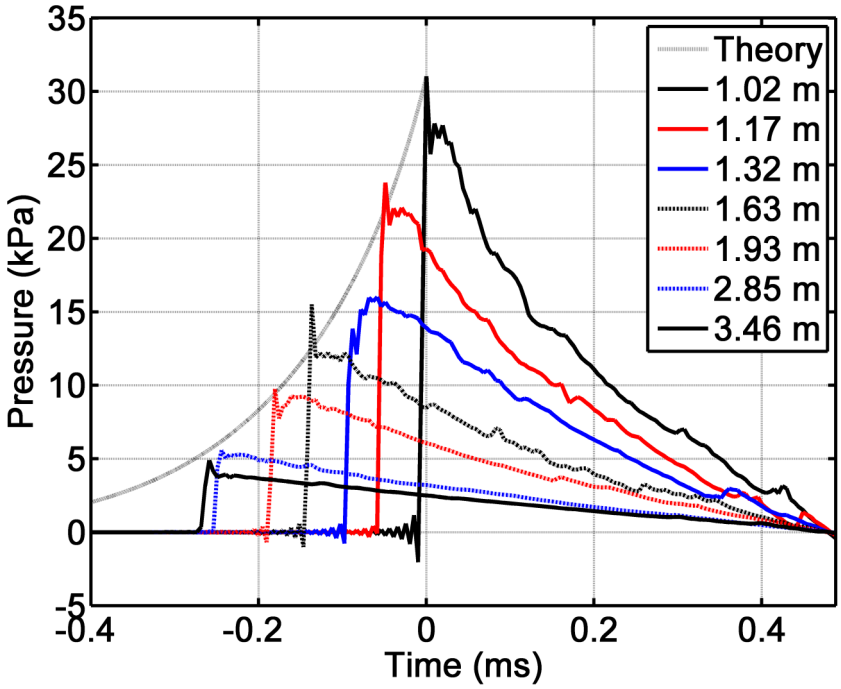

Figure 3.4 Measured waveforms of the acetylene-oxygen balloon compared with the theoretical evolution of the shock amplitude and time.

A useful detail that can be gleaned from Fig. 3.4 is the lengthening of the waveform, seen by the longer time taken from the initial shock to the first zero crossing. The closest microphone shows that it takes just less than 0.5 ms until the initial crossing, while the farthest microphone takes about 0.8 ms. As spherical spreading only affects the amplitude of a waveform, this spreading is best explained by nonlinear propagation theory.

The pedagogical nature of Figs. 3.1 and 3.3 is enhanced when compared with results from the hydrogen-oxygen balloon. In contrast to the shock that was formed with the acetylene-oxygen balloon the hydrogen-oxygen balloon has a much more gradual transition from ambient pressure to the waveform peak. It has been already noted in discussion of Fig. 3.2 that the same time-scale elongation observed in the acetylene-oxygen explosion is not observed in the hydrogen-

oxygen explosion. However, one can still use these latter results to observe nonlinear behavior and distinguish it from the weak shock-like behavior of the acetylene-oxygen balloon.

To more clearly examine the nonlinear evolution of the time waveform for the hydrogen-oxygen balloon in Fig. 3.2, the waveforms of the closest and farthest microphones were multiplied by the respective distances from the sources, thereby removing spherical spreading. The positive portions of the resultant waveforms are shown in Fig. 3.5. Notice the consistency of the location of the zero crossings before and after the initial compression wave combined with advancement of the greater amplitude portions forward in time. This clearly shows nonlinear steepening of the hydrogen-oxygen waveform, but in the preshock region, which is very different nonlinear behavior than the acetylene-oxygen balloon exhibits. Students could also compare results similar to Fig. 3.5 with the Earnshaw solution to examine the dependence of nonlinearity on the nature of the geometric spreading. In this case, the nonlinear distortion of the peak pressure that occurs at approximately -1.0 ms is about half what it would be if the propagation of the wave were planar rather than spherical.

Another interesting feature in Fig. 3.5 is the presence of multiple shocks. This demonstrates that shocks may appear in more locations than just at the head of the propagating wave. It can also be seen that the distance between these shocks is decreasing as the wave propagates and the larger shock will eventually overtake the smaller one. This can be used to introduce the concept of shock coalescence to a class. However, a detailed discussion of shock coalescence is beyond the scope of this article.

The fact that removing spherical spreading effectively normalizes the waveforms in Fig. 3.5 is also evidence that the peak pressure roll-off is not affected by nonlinearity in the pre-shock region, as predicted by the Earnshaw solution. This is further confirmed in Fig. 3.6, where the measured peak pressure closely aligns with linear, spherical geometric spreading theory based on the measured peak pressure at the closest microphone and an assumed source location at the center

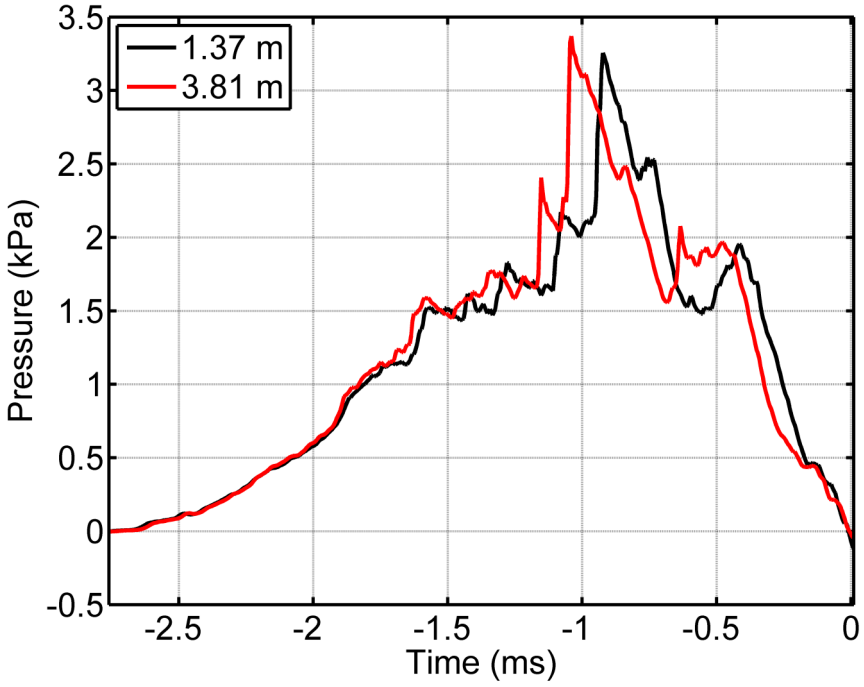

Figure 3.5 Measured waveform of a hydrogen-oxygen balloon from Fig. 3.2 at the closest and farthest microphones with spherical spreading removed.

of the balloon.

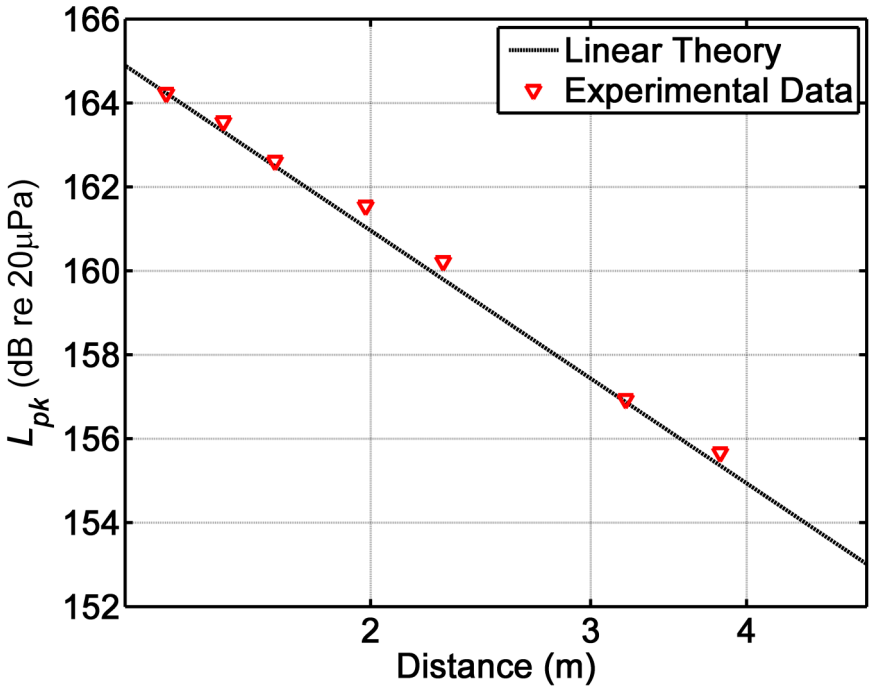

Figure 3.6 Peak measured pressure levels (L_{pk}) of the hydrogen-oxygen balloon with linear theory, confirming data were taken in the pre-shock region.

Chapter 4

High-Speed Video

High speed video was taken of the explosions described in the previous chapter. The camera that was used was a Photron FASTCAM SA2. For the acetylene-oxygen balloon (Fig. 4.1) the frame rate was 15,000 frames per second (fps) and 10,000 fps for the hydrogen-oxygen balloon (Fig. 4.2). The exposure time per frame for both balloons was 1/500,000 s.

There are a few insights that can be gleaned from these videos. Notice that the acetylene and oxygen balloon's reaction is so rapid and explosive that the explosion bursts the back end of the balloon. This allows for a much more uniform spherical impulse. Compare this with the hydrogen-oxygen balloon: the explosion is guided by the unwrapping of the balloon (albeit sped up by the explosion). These features lead one to the conclusion that the acetylene and oxygen balloon's impulse would be quite spherically symmetric while the hydrogen and oxygen balloon's would be cylindrically symmetric. The symmetry of both of these balloons has been verified by Gee, et al. [22]

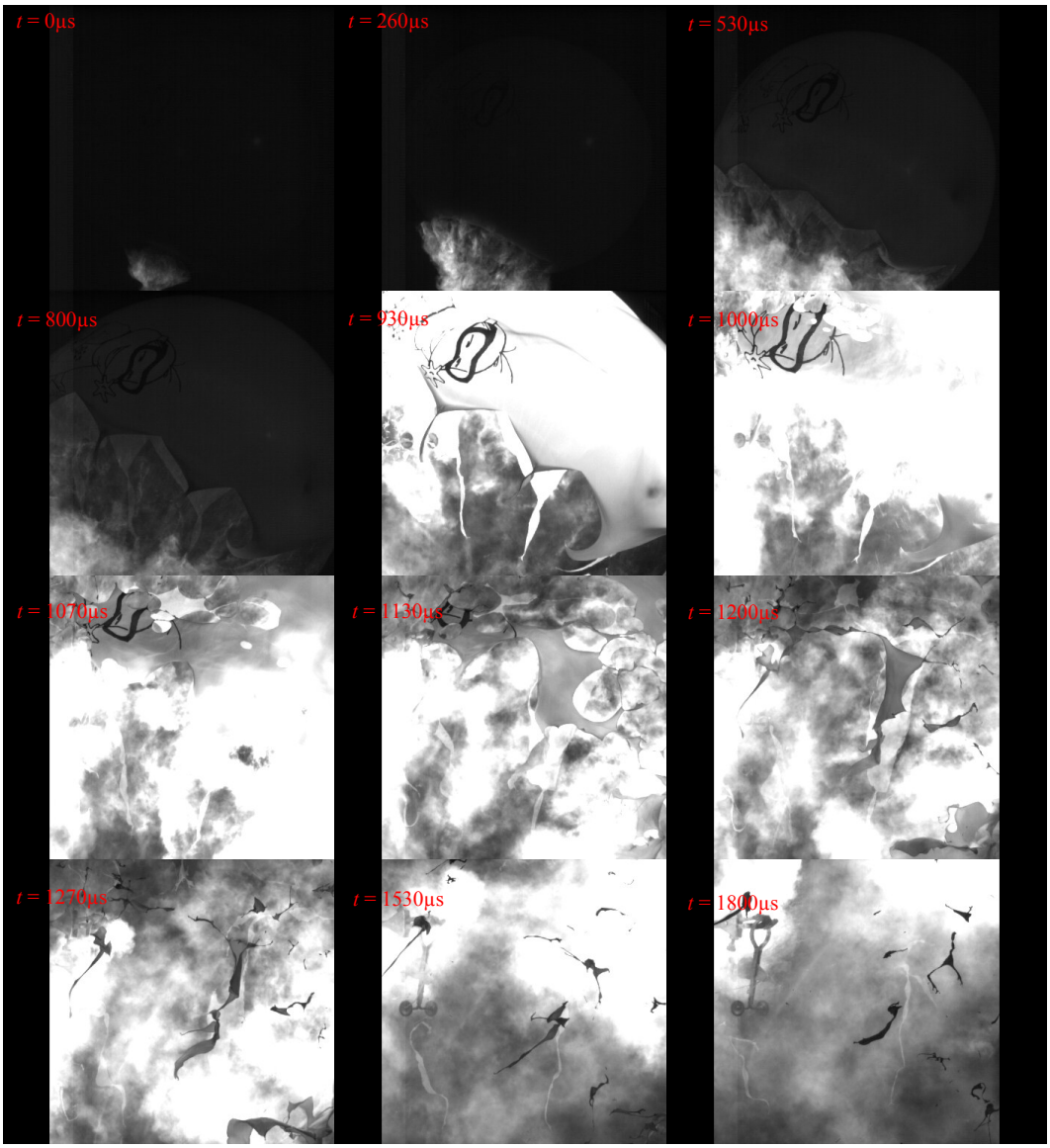

Figure 4.1 Highlights of high-speed video of the acetylene-oxygen balloon explosion. The frame rate is 15,000 fps.

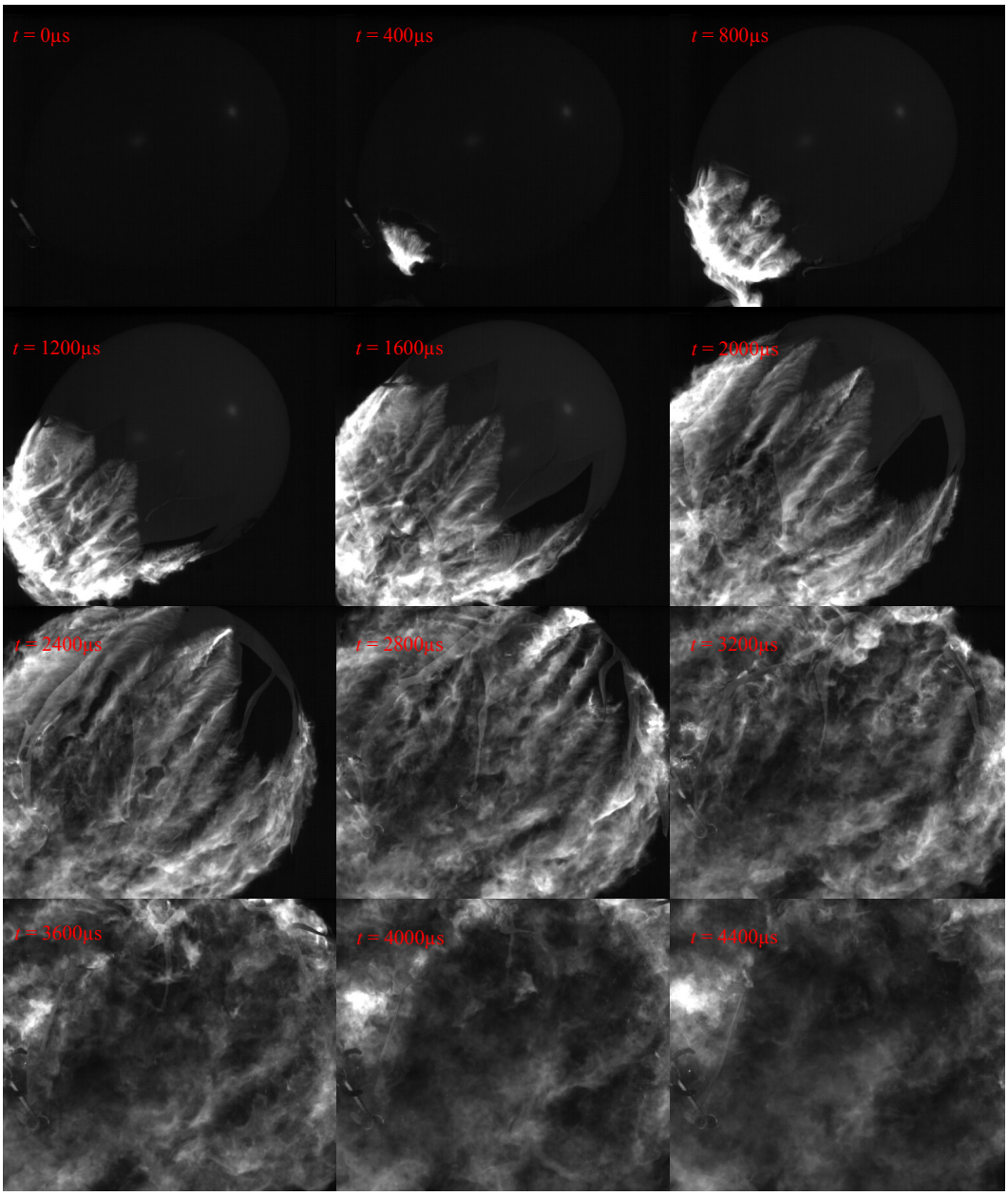

Figure 4.2 Highlights of high-speed video of the hydrogen-oxygen balloon explosion. The frame rate is 10,000 fps.

Chapter 5

Conclusion

This thesis has shown that the explosion from a balloon filled with acetylene and oxygen is a clear demonstration of important nonlinear phenomena, namely dissipation at shocks and waveform spreading. Use of the Earnshaw solution to the lossless Burgers' equation and weak-shock theory allows for a reasonable quantitative prediction of the evolution of waveform characteristics. It has also been shown for comparison that using the explosion from a balloon filled with hydrogen and oxygen is another example where nonlinear theory aids the analysis of the wave propagation through showing waveform steepening. Examination of high speed video yields a qualitative feel for directionality of these finite amplitude impulses as well as for entertainment. Appropriate use of this demonstration should provide the advanced student in physical acoustics an engaging active learning experience in the mathematics of nonlinear phenomena.

Bibliography

[1] W. D. Hayes and J. H. L. Runyan, "Sonic-boom propagation through a stratified atmosphere," J. Acoust. Soc. Am. **51,** 695–701 (1970).

[2] K. L. Gee, V. W. Sparrow, M. M. James, J. M. Downing, C. M. Hobbs, T. B. Gabrielson, and A. A. Atchley, "The role of nonlinear effects in the propagation of noise from high-power jet aircraft," J. Acoust. Soc. Am. **123,** 4082–4093 (2008).

[3] W. E. Baker, *Explosions in Air* (University of Texas Press, Austin and London, 1973), p. 5.

[4] M. Shaw and K. L. Gee, "Acoustical analysis of an indoor test facility for a 30-mm Gatling gun," J. Acoust. Soc. Am. **125,** 2493–2493 (2009).

[5] L. Howle, D. G. Schaeffer, M. Shearer, and P. Zhong, "Lithotripsy: The treatment of kidney stones with shock waves," SIAM Review **40,** 356–371 (1998).

[6] R. O. Cleveland and O. A. Sapozhnikov, "Modeling elastic wave propagation in kidney stones with application to shock wave lithotripsy," J. Acoust. Soc. Am. **118 (4),** 2667–2676 (2005).

[7] D. T. Blackstock, M. F. Hamilton, and A. D. Pierce, in *Nonlinear Acoustics*, M. F. Hamilton and D. T. Blackstock, eds., (University of Texas Press, Austin and London, 1973), Chap. 4, p. 5.

[8] F. M. Pestorius and D. T. Blackstock, in *Finite-Amplitude Wave Effects in Fluids*, L. Bjorno, ed., (IPC Science and Technology Press, Guildfrod, Surrey, England, 1973), pp. 24–29.

[9] H. E. Bass, R. Raspet, J. P. Chambers, and M. Kelly, "Modification of sonic boom wave forms during propagation from the source to the ground," J. Acoust. Soc. Am. **111,** 481–486 (2002).

[10] D. T. Blackstock, "Connection between the Fay and Fubini solutions for plane sound waves of finite amplitude," J. Acoust. Soc. Am. **39,** 1019–1026 (1966).

[11] H. W. Liepmann and A. Roshko, *Elements of Gasdynamics* (Dover Publications, 2002), pp. 57–61.

[12] S. Temkin, "Attenuation of guided, weak sawtooth waves," J. Acoust. Soc. Am. **46,** 267–271 (1968).

[13] D. T. Blackstock, "Propagation of Plane Sound Waves of Finite Amplitude in Nondissipative Fluids," J. Acoust. Soc. Am. **34,** 9–30 (1962).

[14] F. M. Pestorius and S. B. Williams, "Upper limits of weak-shock theory," J. Acoust. Soc. Am. **55,** 1334–1335 (1974).

[15] P. H. Rogers, "Weak-shock solution for underwater explosive shock waves," J. Acoust. Soc. Am. **62,** 1412–1419 (1977).

[16] D. T. Blackstock, "Propagation of a Weak Shock Followed by a Tail of Arbitrary Waveform," In *Proceedings, 11th Int. Cong. Acoustics, Paris, France*, **1,** 305–308 (Paris, 1983).

[17] R. M. Corless, G. H. Gonnet, D. E. G. Hare, D. J. Jeffrey, and D. E. Knuth, "On the Lambert W Function," Advances Comp. Math **5,** 329–359 (1996).

[18] H. E. Bass, L. C. Sutherland, and A. J. Zuckerwar, "Atmospheric absorption of sound: Update," J. Acoust. Soc. Am. **88,** 2019–2021 (1990).

[19] H. E. Bass, L. C. Sutherland, and A. J. Zuckerwar, "Erratum: Atmospheric absorption of sound: Further developments," J. Acoust. Soc. Am. **99,** 1259 (1996).

[20] D. T. Blackstock, "Generalized Burgers equation for plane waves," J. Acoust. Soc. Am. **77,** 2050–2053 (1985).

[21] M. F. Hamilton, Y. A. Il'inskii, and E. A. Zabolotskaya, in *Nonlinear Acoustics*, M. F. Hamilton and D. T. Blackstock, eds., (University of Texas Press, Austin and London, 1973), Chap. 5.

[22] K. L. Gee, J. A. Vernon, and J. H. Macedone, "Auditory risk of exploding hydrogen-oxygen balloons," J. Chem. Ed. (2010).

[23] W. J. Murphy and R. L. Tubbs, "Assessment of noise exposure for indoor and outdoor firing ranges," J. Occup. Environ. Hyg. **4,** 688–697 (2007).

[24] T. B. Gabrielson, T. M. Marston, and A. A. Atchley, "Nonlinear propagation modeling: Guidelines for supporting measurements," In *Proc. Noise-Con*, **114,** 275–285 (2005).

[25] G. R. Price and S. Wansack, "Hazard from an intense midrange impulse," J. Acoust. Soc. Am. **86,** 2185–2191 (1989).

Appendix A

Derivation of the Earnshaw Solution

The lossless Burgers' equation can be written as

$$\frac{\partial p}{\partial x} = \eta p \frac{\partial p}{\partial \tau}. \tag{A.1}$$

where $\eta = \beta/\rho_0 c_0^3$. Let $\phi = \tau + \eta x p$ and $z = x$. Then we have

$$\frac{\partial \phi}{\partial x} = \eta p + \eta x \frac{\partial p}{\partial x}, \tag{A.2}$$

$$\frac{\partial \phi}{\partial \tau} = 1 + \eta x \frac{\partial p}{\partial \tau}, \tag{A.3}$$

$$\frac{\partial z}{\partial x} = 1, \tag{A.4}$$

$$\frac{\partial z}{\partial \tau} = 0. \tag{A.5}$$

Changing the variables requires that the derivatives be modified:

$$\frac{\partial}{\partial x} = \frac{\partial \phi}{\partial x}\frac{\partial}{\partial \phi} + \frac{\partial z}{\partial x}\frac{\partial}{\partial z}, \tag{A.6}$$

$$\frac{\partial}{\partial \tau} = \frac{\partial \phi}{\partial \tau}\frac{\partial}{\partial \phi} + \frac{\partial z}{\partial \tau}\frac{\partial}{\partial z}. \tag{A.7}$$

Combining Eqs. (A.2)-(A.5) with Eqs. (A.6) and (A.7) yields

$$\frac{\partial p}{\partial x} = \frac{\partial \phi}{\partial x}\frac{\partial p}{\partial \phi} + \frac{\partial z}{\partial x}\frac{\partial p}{\partial z} = \eta \left(p + x \frac{\partial p}{\partial x} \right) \frac{\partial p}{\partial p} + \frac{\partial \phi}{\partial z} \tag{A.8}$$

$$\Rightarrow \frac{\partial p}{\partial x}\left(1-\eta x\frac{\partial p}{\partial \phi}=\eta p\frac{\partial p}{\partial \phi}\right)+\frac{\partial p}{\partial z} \tag{A.9}$$

$$\Rightarrow \frac{\partial p}{\partial x}=\frac{\eta p\frac{\partial p}{\partial \phi}+\frac{\partial p}{\partial z}}{1-\eta x\frac{\partial p}{\partial \phi}}=\frac{\eta p\frac{\partial p}{\partial \phi}}{1-\eta z\frac{\partial p}{\partial \phi}}+\frac{\frac{\partial p}{\partial z}}{1-\eta z\frac{\partial p}{\partial \phi}}, \tag{A.10}$$

and

$$\frac{\partial p}{\partial \tau}=\frac{\partial \phi}{\partial \tau}\frac{\partial p}{\partial \phi}+\frac{\partial z}{\partial \tau}\frac{\partial p}{\partial z}=\left(1+\eta x\frac{\partial p}{\partial \tau}\right)\frac{\partial p}{\partial \phi} \tag{A.11}$$

$$\Rightarrow \frac{\partial p}{\partial \tau}\left(1-\eta x\frac{\partial p}{\partial \phi}\right)=\frac{\partial p}{\partial \phi} \tag{A.12}$$

$$\Rightarrow \frac{\partial p}{\partial \tau}=\frac{\frac{\partial p}{\partial \phi}}{1-\eta x\frac{\partial p}{\partial \phi}}=\frac{\frac{\partial p}{\partial \phi}}{1-\eta z\frac{\partial p}{\partial \phi}}. \tag{A.13}$$

Inserting Eqs. (A.10) and (A.13) into the Burgers' equation yields

$$\frac{\eta p\frac{\partial p}{\partial \phi}}{1-\eta z\frac{\partial p}{\partial \phi}}+\frac{\frac{\partial p}{\partial z}}{1-\eta z\frac{\partial p}{\partial \phi}}=\frac{\eta p\frac{\partial p}{\partial \phi}}{1-\eta z\frac{\partial p}{\partial \phi}} \tag{A.14}$$

$$\Rightarrow \frac{\frac{\partial p}{\partial z}}{1-\eta z\frac{\partial p}{\partial \phi}}=0 \tag{A.15}$$

$$\Rightarrow \frac{\partial p}{\partial z}=0 \tag{A.16}$$

$$\Rightarrow p=f(\phi), \tag{A.17}$$

which is the Earnshaw solution.

Appendix B

Peak Shock Pressure and Location

The derivation below follows the method Blackstock used. [16]

Begin with the planar Earnshaw solution to the lossless Burgers' equation (Eqs. (1.1,1.2,1.3)). The Burgers' equation is given here for reference:

$$\frac{\partial p}{\partial x} = \frac{\beta}{\rho_0 c_0^3} p \frac{\partial p}{\partial \tau}, \tag{B.1}$$

with pressure p, distance x, parameter of nonlinearity β, the ambient air density ρ_0, small signal sound speed c_0, and retarded time $\tau = t - x/c_0$, with time t. For simplification, the pressure is nondimensionalized, and the Earnshaw solution is written as

$$V \equiv \frac{p}{p_0} = f(\phi), \tag{B.2}$$

$$\phi = \tau + \frac{\beta p_0 x}{\rho_0 c_0^3} V. \tag{B.3}$$

See Appendix A for details.

In terms of the nondimensional pressure weak shock theory gives the following relation:

$$\frac{\partial \tau_{sh}}{\partial x} = -\frac{\beta p_0}{\rho_0 c_0^3} \frac{V_a + V_b}{2}, \tag{B.4}$$

where V_a is the normalized pressure just ahead of the shock, V_b is the normalized pressure just behind the shock, and τ_{sh} is the retarded time of arrival of the shock. Fortunately, the pressure just ahead of the shock is identically zero, as stated above, so V_a can be ignored.

To simplify this discussion, the substitution of $\alpha = \beta p_0/\rho_0 c_0^3$ is made.

In order to solve Eqs. (B.2 - B.4) simultaneously, differentiate Eq. (B.3) with respect to x and evaluate at τ_{sh}, then reorganize as follows:

$$\frac{\partial \phi_{sh}}{\partial x} = \frac{\partial \tau_{sh}}{\partial x} + \alpha \left(V_{sh} + x\frac{V_{sh}}{2} \right), \tag{B.5}$$

$$\Rightarrow \frac{\partial \tau_{sh}}{\partial x} = \frac{\partial \phi_{sh}}{\partial x} - \alpha \left(V_{sh} + x\frac{V_{sh}}{2} \right), \tag{B.6}$$

where $\phi_{sh} = \phi|_{\tau=\tau_{sh}}$ and $V_{sh} = V_b$ is the peak pressure of the shock. Equate Eq. (B.5) with Eq. (B.4):

$$\frac{\partial \phi_{sh}}{\partial x} - \alpha \left(V_{sh} + x\frac{V_{sh}}{2} \right) = -\alpha \frac{V_{sh}}{2}. \tag{B.7}$$

Now multiply Eq. (B.7) by $\partial x/\partial \phi_{sh}$ and by $2V_{sh}$, simplify, reorganize, and then integrate:

$$1 - V_{sh}\alpha \frac{\partial x}{\partial \phi_{sh}} - x\alpha \frac{\partial V_{sh}}{\partial \phi_{sh}} = -\alpha \frac{V_{sh}}{2} \frac{\partial x}{\partial \phi_{sh}}, \tag{B.8}$$

$$2V_{sh} - 2\alpha V_{sh}^2 \frac{\partial x}{d\phi_{sh}} - 2x\alpha V_{sh} \frac{\partial V_{sh}}{\partial \phi_{sh}} = -\alpha V_{sh}^2 \frac{\partial x}{\partial \phi_{sh}}, \tag{B.9}$$

$$\alpha \left(V_{sh}^2 \frac{\partial x}{\partial \phi_{sh}} + 2xV_{sh} \frac{\partial V_{sh}}{\partial \phi_{sh}} \right) = 2V_{sh}, \tag{B.10}$$

$$x\alpha V_{sh}^2 = \int 2V_{sh} d\phi_{sh} = 2\int_0^{\phi_{sh}} f(\phi) d\phi. \tag{B.11}$$

The exponential tail is given by $f(t) = \exp(-t/t0)$. Inserting this relation into Eq. (B.11) yields

$$x\alpha V_{sh}^2 = 2\int_0^{\phi_{sh}} e^{-\phi/t_0} \phi = 2t_0 \left(1 - e^{-\phi_{sh}/t_0} \right) = 2t_0 \left(1 - V_{sh} \right). \tag{B.12}$$

This can be solved for V_{sh} via the quadratic equation:

$$x\alpha V_{sh}^2 + 2t_0 V_{sh} - 2t_0 = 0, \tag{B.13}$$

$$\Rightarrow V_{sh} = \frac{-2t_0 \pm \sqrt{4t_0^2 p_0^2 + 8x\alpha t_0}}{2x\alpha} = \frac{\pm\sqrt{1+2bx}-1}{bx}, \tag{B.14}$$

where the substitution of $b = \alpha/t_0 = \beta p_0/t_0\rho_0 c_0^3$ is implemented.

The physical interpretation of the plus or minus sign is the direction of propagation. The plus implies outgoing (positive) propagation and the minus incoming (negative) propagation. Only outgoing propagation is considered here, so only the positive case is dealt with below. Then the peak shock pressure as a function of distance is

$$p_{sh} = p_b = p_0 \frac{\sqrt{1+2bx}-1}{bx}. \tag{B.15}$$

Expanding b in Eq. (B.15) yields Eq. (1.14):

$$p_{sh} = \frac{\sqrt{1+2p_0 Cx/t_0}-1}{Cx/t_0}. \tag{B.16}$$

(Recall that $C = \beta/\rho_0 c_0^3 = b \cdot t_0/p_0$.)

Once p_{sh} is found, Eqs. (1.2, 1.3) evaluated at ϕ_{sh} allow τ_{sh} to be found:

$$p = p_0 e^{-\phi/t_0} \Rightarrow \phi = -t_0 \ln(p/p_0), \tag{B.17}$$

$$\tau = \phi - t_0 bxp/p_0 = -t_0 \left[\ln(p/p_0) + bxp/p_0\right], \tag{B.18}$$

$$\tau_{sh} = -t_0 \left[\ln(p_{sh}/p_0) + bxp/p_0\right] = -t_0 \ln\left(\frac{\sqrt{1+2bx}-1}{bx/p_0}\right) - t_0\sqrt{1+2bx} + t_0. \tag{B.19}$$

Equation (B.19) expands to Eq. (1.15):

$$\tau_{sh} = t_0 - t0\sqrt{1+2p_0 Cx/t_0} - t_0 \ln\left(\frac{\sqrt{1+2p_0 Cx/t_0}-1}{p_0 Cx/t_0}\right). \tag{B.20}$$

Index